PAPER • OPEN ACCESS

Dominant acceptors in Li doped, magnetron deposited Cu$_2$O films

To cite this article: M Nyborg *et al* 2021 *Mater. Res. Express* **8** 125903

View the article online for updates and enhancements.

Materials Research Express

PAPER

OPEN ACCESS

Dominant acceptors in Li doped, magnetron deposited Cu$_2$O films

M Nyborg* , K Karlsen , K Bergum and E Monakhov*

Physics Department/Centre for Materials Science and Nanotechnology, University of Oslo, PO Box 1048 Blindern, Oslo N-0316, Norway
* Authors to whom any correspondence should be addressed.

E-mail: martin.nyborg@fys.uio.no and eduard.monakhov@fys.uio.no

Abstract

Cu$_2$O films deposited by reactive magnetron sputtering with varying Li concentrations have been investigated by a combination of temperature-dependent Hall effect measurement and thermal admittance spectroscopy. As measured by secondary ion mass spectrometry, Li concentrations up to 5×10^{20} Li/cm^3 have been achieved. Li doping significantly alters the electrical properties of Cu$_2$O and increases hole concentration at room temperature for higher Li concentrations. Moreover, the apparent activation energy for the dominant acceptors decreases from around 0.2 eV for undoped or lightly doped Cu$_2$O down to as low as 0.05 eV for higher Li concentrations.

1. Introduction

Cuprous oxide (Cu$_2$O) is an attractive p-type semiconductor widely investigated for its possible application in photovoltaics. It has intriguing properties suitable for both single- and tandem-junction solar cells. Cu$_2$O has a direct bandgap of 2.17 eV, is non-toxic, has high natural abundance, and has the potential for low-cost production schemes. The Shockley–Queisser limit is about 20% for a single junction and could reach over 30% in a tandem junction configuration [1–3]. Thick oxidized copper sheets have had steep progress in the past years, achieving efficiencies as high as 8% [4]. However, thin-film devices have demonstrated considerably lower performance [5, 6]. Among the possible reasons for the low efficiencies of the solar cells based on Cu$_2$O, one can point to a lack of control over the carrier concentration and the inability to synthesize n-type Cu$_2$O that would enable a p-n homojunction [7–9].

Thin-film Cu$_2$O cells suffers from poor carrier collection, especially at higher wavelengths, which could be attributed to the relative low mobility and recombination at the interface and within the Cu$_2$O layer [9, 10] Brandt *et al* [11] suggests that thermal and chemical treatments will be needed to reduce or passivate defects in order to improve cell performance of Cu$_2$O devices. The persistent p-type nature of Cu$_2$O is believed to be due to the acceptor states of copper vacancies (V$_{Cu}$), which is substantiated by the studies of their configurations and electronic properties by density functional theory (DFT) [12]. Thus, the control over carrier concentration should involve the ability to control the V$_{Cu}$ concentration or to passivate V$_{Cu}$.

Perhaps, the most prominent candidates for passivating V$_{Cu}$ and potential n-type doping are Group-I elements. For example, hydrogen atoms are predicted to form stable complexes with V$_{Cu}$ (H–V$_{Cu}$) [13]. Although H–V$_{Cu}$ is still an acceptor, the acceptor level has an activation energy of around 1.2 eV, which effectively reduces the acceptor activity of V$_{Cu}$. Isolated hydrogen atoms are predicted to occupy an interstitial position (H$_i$). The donor level of H$_i$ is expected to lie deep in the bandgap, at around E$_V$ + 1 eV, where E$_V$ is the valence band edge. Introducing atomic hydrogen can, thus, moderate the hole concentration in Cu$_2$O.

Similar to hydrogen, alkali metals, such as Li and Na, can also be considered for carrier concentration control. Theoretical predictions on the electronic activity of these metals are, however, scarce. *Isseroff and Carter* [14] have performed DFT calculations on the interaction of several metals, such as Li, Mg, Mn, and Za, with V$_{Cu}$ and electronic properties of their complexes. It is established that the complex of Li and V$_{Cu}$ (Li–V$_{Cu}$) has no electronic levels in the bandgap. Moreover, Li–V$_{Cu}$ has the lowest formation energy among the complexes considered in the study. It has been concluded that Li has the greatest potential to passivate V$_{Cu}$ and to improve the electronic properties of Cu$_2$O.

Table 1. Li concentration and film thickness in the prepared samples deduced from SIMS measurements.

Sample #	Li concentration (cm^{-3})	Film thickness (nm)
1 (undoped)	$<10^{15}$	470
2	2×10^{18}	485
3	7×10^{18}	550
4	2×10^{20}	560
5	5×10^{20}	530

Perhaps, the first systematic study of the effect of alkali metal on conductivity and carrier concentration in Cu_2O has been performed by Minami *et al* [15] for Na. In that study, Cu_2O was prepared by oxidizing metallic Cu sheets, and Na was introduced by in-diffusion from the surface. It has been observed that conductivity and carrier concentration increases with the duration and the temperature of the Na in-diffusion. For instance, the carrier concentration at room temperature has increased from 10^{13} cm^{-3} (for undoped Cu_2O) to 10^{19} cm^{-3} (after the longest Na in-diffusion). Moreover, Temperature-dependent Hall effect (TDH) measurements have revealed a decrease in the activation energy of the acceptors: from 0.15 eV (for undoped Cu_2O) down to 0.02 eV (for Cu_2O with hole concentration of 4×10^{17} cm^{-3} at room temperature). The samples with the longest Na in-diffusion exhibited degenerated p-type conduction. This is a surprising result since Na, similar to Li, is expected to passivate V_{Cu} and reduce hole concentration. The observed increase in hole concentration was attributed to an excess formation of V_{Cu} compensating for Na atoms incorporated at the interstitial site as donors [15]. Such an interpretation, however, cannot explain the decrease in the acceptor activation energy, since the acceptor activation energy of V_{Cu} is believed to be ~0.2 eV [12].

Recently, it has been reported on the effect of Li on resistivity and carrier concentration in magnetron sputter deposited Cu_2O films [16]. It is observed a trend similar to that reported by Minami *et al* [15] for Na: the hole concentration increases for higher Li content. The undoped Cu_2O films exhibit a hole concentration of 10^{15} cm^{-3}, while those doped with Li demonstrate a hole concentration of up to 10^{17} cm^{-3} at room temperature.

In this study, we report on the electronic properties of the dominant acceptors in Li doped, magnetron sputter deposited Cu_2O films. For the first time temperature dependence of hole concentration and the activation energy of the dominant acceptors are deduced using TDH measurements and thermal admittance spectroscopy (TAS) on Li doped Cu_2O.

2. Experimental

500 nm thick Cu_2O films with various Li content were deposited by reactive DC and RF magnetron co-sputtering from Cu (4N, AEM Inc.) and Cu:Li targets (4N 99:1 wt% AEM Inc. and 4N 99.99:0.01 wt% AEM Inc.) in a Semicore Triaxis system. Two 1×1 cm^2 substrates were used in each deposition run: (i) an UV-grade fused silica substrate with a resistivity of >1 GOhm-cm for TDH measurements and (ii) a n-type Si substrate for TAS. The Si substrates were cut from an n-type (100) Si wafer with a resistivity of 5 Ohm-cm. The n-type Si was chosen in order to form a p-n heterojunction between Cu_2O and Si. The fused silica substrates were cleaned for 1 min in Pirhana solution, rinsed in DI water, then subsequently ultrasonically washed for 5 min in isopropanol before deposition. The Si substrates was prepared following the RCA procedure. Chamber base pressure was lowered to below 2.7×10^{-4} PA, subsequently the targets were pre sputtered for 20 min before initiating deposition for 15 min at 400 °C. A total of 10 samples were prepared after 5 depositions for different Li content. Additional details on deposition and characterization of Li doped Cu_2O is reported elsewhere [16].

Secondary ion mass spectrometry (SIMS) was used to measure Li concentration in the films. Table 1 shows the Li concentration and film thickness in the samples studied.

Charge carrier density has been assessed by TDH measurements with a Lakeshore 7604 setup in the temperature range 95–550 K, employing a field strength of ±1 T. Two separate cryostats were used for the TDH measurements: (1) a low-temperature one in the rage 95–300 K and (2) a high-temperature one in the range 300–550 K. The measurements were performed in the Van der Pauw geometry.

Diodes for TAS measurements were defined on the samples with the Si substrates by a lift-off lithography process, which involved (i) deposition of 400 nm thick Au front contacts with a diameter of 1.5 mm on the Cu_2O film and (ii) subsequent etching of Cu_2O around the Au contacts. Al was deposited as a back contact, resulting in Au/Li:Cu_2O/n-Si/Al structures. Current-voltage measurements confirmed a diode behavior of the structures with a rectification of 2–6 orders of magnitude. TAS was performed with an Agilent 4280A LCR meter under a reverse bias of −1 V, using a probing ac signal with frequencies between 1 kHz to 1 MHz and an amplitude of 20 mV.

Table 2. Some of the main parameters for the Cu$_2$O film used in the simulation.

Parameter	Value	References
Band gap [eV]	2.17	[12]
Relative permittivity [eV]	7.11	[12]
Electron affinity [eV]	3.1	[12]
Film thickness [nm]	550	table 1, sample #3
Acceptor concentration [cm^{-3}]	1×10^{18}	figure 1(a), sample #3
Acceptor activation energy [eV]	0.14	figure 3, sample #3

Device simulation of the pn-junction was performed using Silvaco TCAD device simulator. The device structure and parameters were chosen to corroborate with the experimental data, the Si substrate was defined with a n-type doping concentration of 10^{15} cm^{-3}. See table 2 for the main material parameters used in the simulation.

3. Results and discussion

3.1. Temperature-dependent hall effect

Hall effect measurements, performed for the Cu$_2$O films deposited on the quartz substrates, from the polarity of the Hall voltage it is revealed p-type conductivity in all the samples [17]. At room temperature, the hole concentration in the films is in the range 10^{15}–10^{17} cm^{-3}. The results of the TDH measurements for samples #1-#5 are presented in figure 1. As mentioned above, two separate cryostats were used for temperature ranges 95–300 K and 300–550 K. This can be seen in figure 1(b) as a discontinuity in the temperature dependence for hole mobility at 300 K. Almost no discontinuity between the two cryostats is observed for the hole concentration in figure 1(a).

The hole concentrations (figure 1(a)) show a strong dependence on temperature. For instance, in the undoped film (sample #1) the hole concentration changes from 10^{13} cm^{-3} at around 200 K up to 10^{18} cm^{-3} at 550 K. The temperature-dependent hole concentration for a p-type semiconductor can be described by the following relation [17]:

$$p(\text{T}) \gg \frac{g_a N_v (N_a - N_d)}{N_d} \exp\left(-\frac{\Delta E_a}{kT}\right) \tag{1}$$

where $p(T)$ is the hole concentration, N_a is the acceptor concentration, N_d is the net concentration of the compensating donors, E_a is the activation energy of the acceptor, N_v is the valence band effective density of states, g_a is the degeneracy factor, k is Boltzmann constant, and T is temperature. One can observe that $p(T)$ for sample #1 in figure 1(a) deviates from the simple exponential dependence in equation (1). In the experimental results, the slope of $p(T)$ increases with increasing T. We interpret this as an indication of several acceptor levels in the film, where deeper acceptors become activated at higher T. Nevertheless, we have estimated the activation energy of the most shallow acceptor by fitting equation (1) in the temperature range 200–300 K. The estimated activation energy is ~0.16 eV, as indicated in parentheses in figure 1(a).

Doping with Li results in a noticeable effect on the electronic properties of Cu$_2$O (figure 1(a)). Samples #2 (2×10^{18} Li/cm^3) and #3 (7×10^{18} Li/cm^3) exhibit somewhat lower hole concentrations as compared to sample #1 (undoped). Moreover, the acceptor activation energies appear to increase with Li doping to values of ~0.25 eV and ~0.22 eV for samples #2 and #3, respectively. This observation is consistent with theoretical results by *Isseroff and Carter* [14], where Li is predicted to passivate V$_{Cu}$. Similar to the undoped sample #1, an indication of deeper acceptors can be seen in $p(T)$, which is manifested by steeper slopes of p(T) at higher T. At 550 K, $p(T)$ appears to stabilize at around 10^{18} cm^{-3}.

For higher Li concentrations, however, the effect of Li doping is different. Firstly, the hole concentration at room temperature increases significantly: to around 10^{16} cm^{-3} for sample #4 and to around 10^{17} cm^{-3} for sample #5. At 550 K, the hole concentration appears to saturate at around 10^{18}–10^{19} cm^{-3}. Secondly, the activation energy for the dominating shallow acceptors decreases to 0.12 eV and 0.05 eV for samples #4 and #5, respectively. This observation contradicts the predictions by *Isseroff and Carter* [14] and the trend observed for the lower Li concentration (samples #2 and #3). However, this is in line with the finding by Minami *et al* [15], who observed an increase in the hole concentration and a decrease in the activation energy after Na doping. Since the Li concentration in samples #4 and #5 is relatively high (2×10^{20} Li/cm^3 and 5×10^{20} Li/cm^3), one can speculate that Li with such a high concentration can change the material properties of Cu$_2$O and thus affect
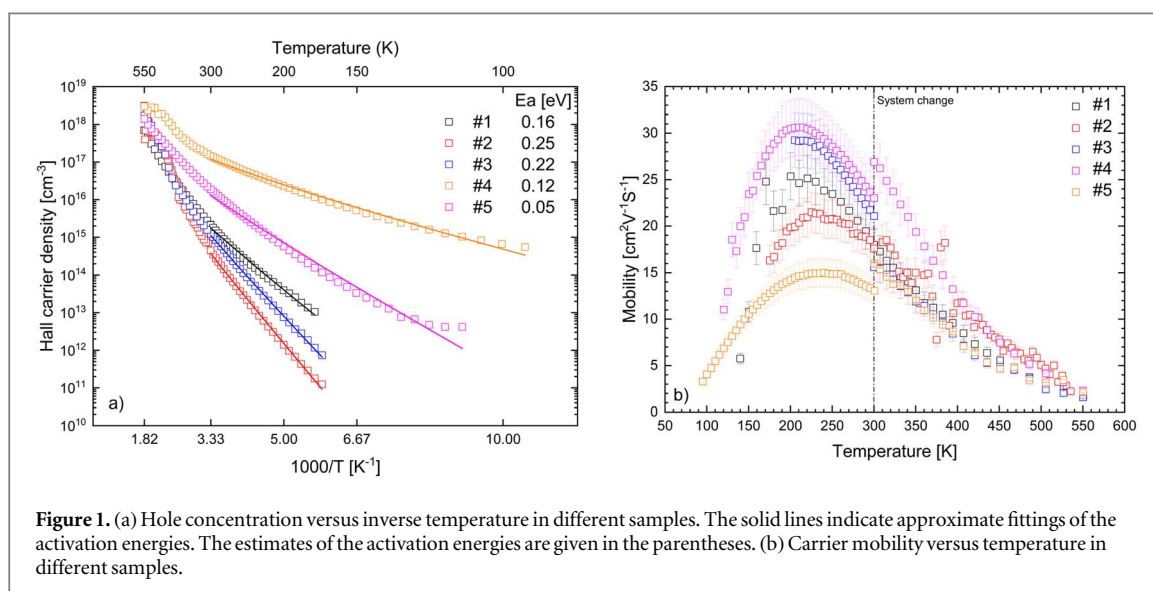
Figure 1. (a) Hole concentration versus inverse temperature in different samples. The solid lines indicate approximate fittings of the activation energies. The estimates of the activation energies are given in the parentheses. (b) Carrier mobility versus temperature in different samples.

the formation energy of defects, including that of V_{Cu}. According to the widely accepted formalism, the equilibrium concentration of a defect in a crystal is defined by the formation energy of the defect [18]. A decrease in the formation energy would lead to an increase in the concentration of V_{Cu} and would affect the acceptor level position in the band gap. In the study by Minami *et al* [15], the concentration of Na in Cu_2O has not been reported. One can speculate, however, that Na concentration could be high, and similar consideration can be applied to the effect of Na.

The temperature dependent mobility data in figure 1(b) show a typical bell-shape temperature dependency. This is generally attributed to the contribution of ionized impurity scattering at low temperatures and intrinsic scattering at elevated temperatures (i.e. phonon scattering) [12]. The mobility is relatively low compared to that reported for single crystal samples ($80–100\ cm^2V^{-1}s^{-1}$) [19], this could be attributed to an increase of neutral impurity scattering and grain boundary scattering in polycrystalline thin films.
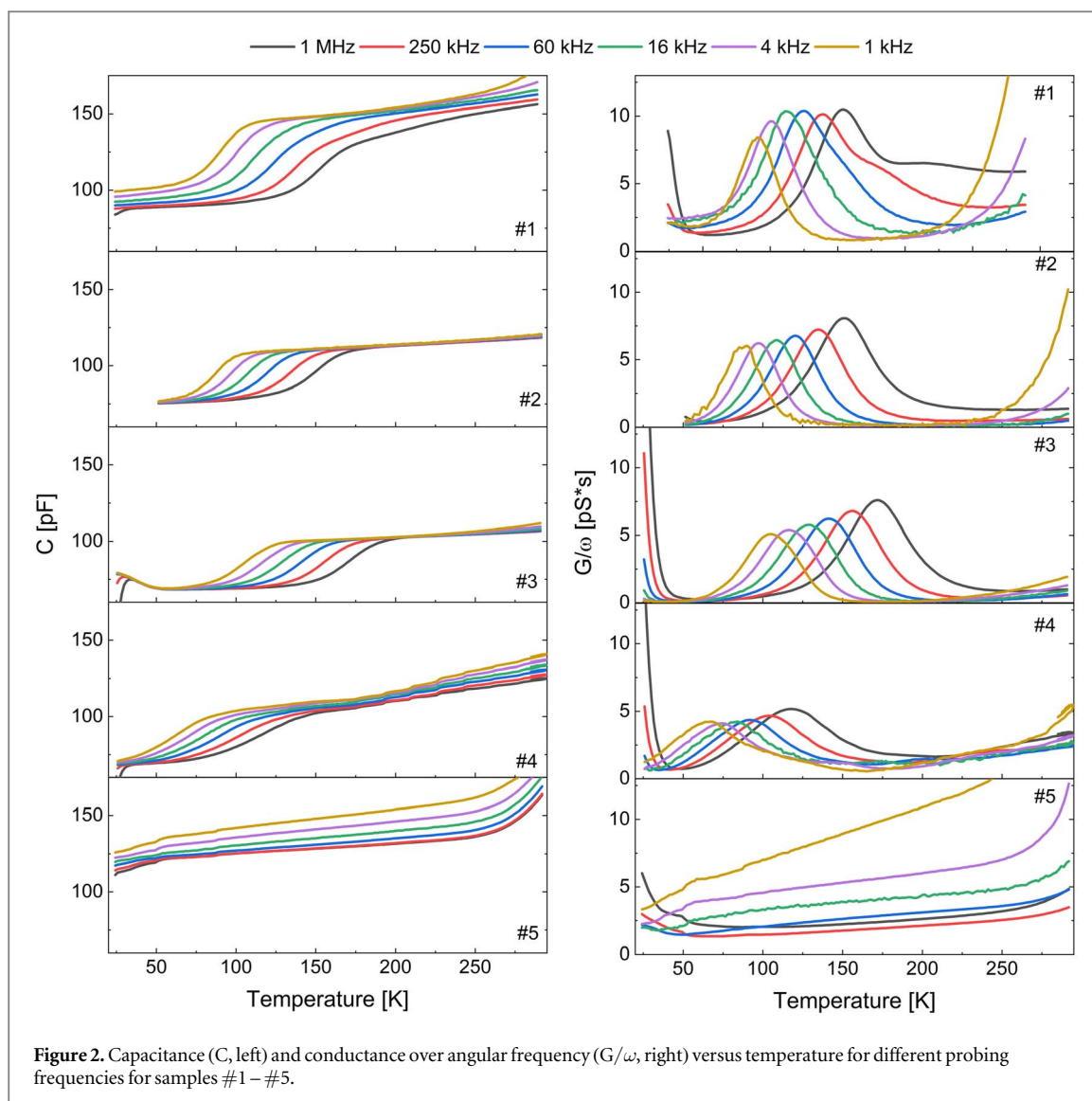
It has not been observed any dependence in the band gap on the film thickness in Li doped Cu_2O [16]. Similarly, no such dependence is observed for the doping concentration. We can conclude that the observed changes in the electronic properties are due to Li doping and are not caused by different film thickness.

3.2. Thermal admittance spectroscopy

TAS measurements have been employed to substantiate the characterization of electrically active defects in the deposited films. As mentioned above, for TAS measurements the Cu_2O films are deposited on n-type Si substrates with a doping concentration of $1 \times 10^{15}\ cm^{-3}$. The structure forms a p-n heterojunction that shows a diode behavior and the corresponding capacitance of the diode. Figure 2 shows the results of TAS for samples #1–#5, where the capacitance (C) and the conductance over the angular frequency (G/ω) are measured at a reverse bias of −1 V and plotted versus temperature for 6 probing frequencies. As established from TDH measurements (figure 1), the acceptors in the Cu_2O films are partially activated at room temperature, which results in a carrier concentration in the range $10^{14}–10^{17}\ cm^{-3}$ (depending on the sample). The total capacitance of the sample is then determined by depletion regions in the film and in the substrate. The value of the total capacitance at room temperature is around 120–150 pF (figure 2, left). As the temperature decreases, the acceptors freeze out and the hole concentration in the Cu_2O film decreases rapidly, as seen in TDH measurements in figure 1(a). In TAS, the freeze-out of the acceptors in the film is manifested as a step-like drop of the capacitance (figure 2, left). In the conductance measurements (figure 2, right), the acceptors freeze-out corresponds to a maximum.

The activation energy of the acceptors can be deduced by performing capacitance and conductance measurements at different probing frequencies. The temperature of the step-like capacitance drop or the conductance maximum depends on the frequency [17]. From the TAS plots (figure 2), a single dominating acceptor freeze-out is observed in samples #1 - #4. By performing a standard Arrhenius analysis (figure 3), the deduced acceptor energies are 0.11 eV, 0.11 eV, 0.14 eV and 0.08 eV for sample #1, #2, #3 and #4, respectively. In sample #5, no clear acceptor freeze-out is visible within the investigated temperature range, which indicates very low activation energy for the acceptors. This is, in fact, consistent with the observation by TDH, where the activation energy for sample #5 (figure 1) is deduced to be as low as 0.05 eV.

Figure 2. Capacitance (C, left) and conductance over angular frequency (G/ω, right) versus temperature for different probing frequencies for samples #1 − #5.
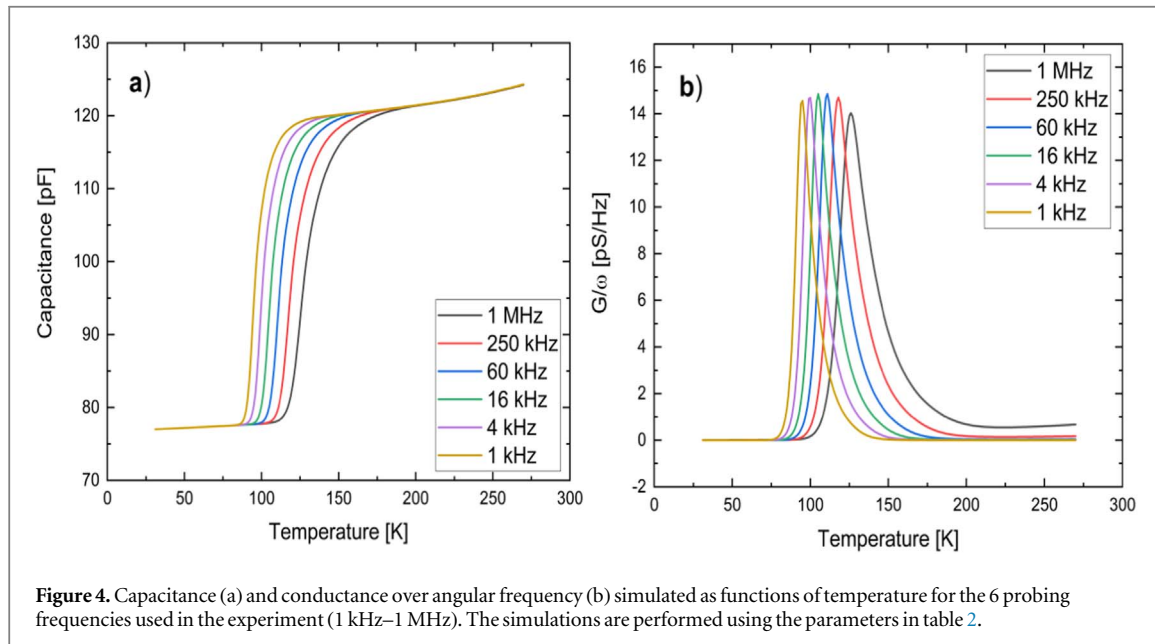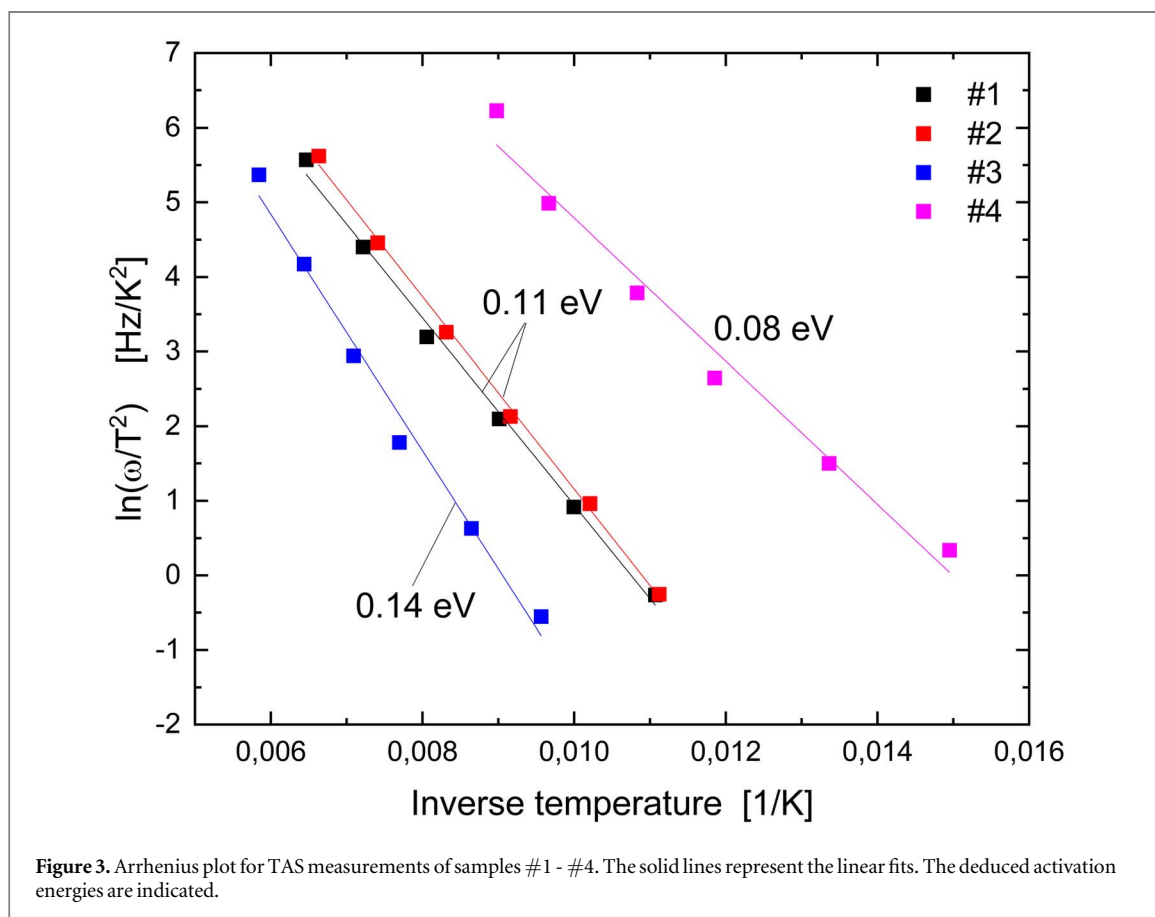
One can see that the activation energies deduced by TAS are systematically lower compared to those deduced by TDH. The reason can be twofold: (1) One can observe that p(T) deviates from perfect exponential dependence in figure 1(a), which introduces uncertainty in the activation energy deduced from the TDH measurements. (2) The Poole-Frenkel effect [20], which lowers the activation energy in external electric fields, can play an important role in the TAS measurements. Indeed, in the TDH measurements, the voltage spans over about 1 cm, resulting in a weak electric field. In the TAS measurements, most of the voltage drop occurs at the p-n heterojunction, which results in a higher electric field in the probing region. In any case, it is clear, however, that the trend for the decreasing activation energy at high Li concentration is similar: the activation energies in samples #4 and #5 are consistently lower compared to other samples.

3.3. TAS simulations

In order to corroborate and substantiate the interpretation of the TAS measurements, we have performed simulations using Silvaco TCAD [21]. Figure 4 shows the simulated capacitance (C) and conductance over the angular frequency (G/ω) as functions of temperature for different frequencies that were used in the experiment (figure 2). The parameters were chosen to illustrate the simulations correspond to those for sample #3, since it represents an intermediate case. Simulations with different parameters, such as film thickness, acceptor activation energy, and acceptor concentration, have been carried out and demonstrated the same trends as in the experiment.

At 270 K, the simulation shows the presence of a depletion region associated with the p-n heterojunction between p-type Cu_2O and n-type Si. Moreover, since the concentration of acceptors in Cu_2O (10^{18} cm^{-3}) is much higher compared to donor concentration in Si (10^{15} cm^{-3}), the depletion region is extended predominantly into Si. This is in full agreement with the theory on the depletion region in p-n junctions [17].

Figure 3. Arrhenius plot for TAS measurements of samples #1 - #4. The solid lines represent the linear fits. The deduced activation energies are indicated.

Figure 4. Capacitance (a) and conductance over angular frequency (b) simulated as functions of temperature for the 6 probing frequencies used in the experiment (1 kHz–1 MHz). The simulations are performed using the parameters in table 2.

Thus, at around room temperature, the capacitance of the structure is determined mainly by the depletion region in Si, which corresponds to around ∼120 pF for the given diode size.

As temperature decreases, the acceptors in the Cu_2O films start to freeze out, which is manifested in the capacitance drop in the TAS measurements. At low temperatures, when the acceptors are completely frozen out, the Cu_2O film becomes a fully depleted dielectric. The total capacitance of the structure is then determined mainly by the capacitance of the depleted film, which corresponds to around ∼80 pF for the given film thickness (table 2) and the diode size. The simulation supports, hence, the interpretation that the capacitance drop and the conductance peak in the TAS measurements correspond to the freeze-out of the dominant acceptors in the Cu_2O film.

4. Conclusion

We have performed Hall effect and TAS investigations of the effect of Li doping on the dominant acceptors in Cu_2O films deposited by reactive DC and RF magnetron sputtering from a metallic Cu target. During the growth, the films were doped with Li by co-sputtering of Cu:Li targets. Li concentrations up to 5×10^{20} Li/cm^3 have been achieved. We observe an increase in hole concentration at room temperature for higher Li concentrations. This can be considered as a counter-intuitive finding since Li is expected to passivate V_{Cu} that is commonly believed to be the main acceptor in Cu_2O. Moreover, the apparent activation energy for the dominant acceptors decreases from around 0.2 eV down to 0.05 eV for higher Li concentrations, as determined by TDH. Our results are, however, in line with literature reports on the effect of other group-I doping: Na.

Acknowledgments

Data availability statement

The data that support the findings of this study are available upon reasonable request from the authors.

ORCID iDs

M Nyborg ⓘ https://orcid.org/0000-0002-2787-9073
K Karlsen ⓘ https://orcid.org/0000-0002-0904-2480
K Bergum ⓘ https://orcid.org/0000-0002-4093-521X
E Monakhov ⓘ https://orcid.org/0000-0002-7015-3358

References

[1] de Vos A 1980 *J. Phys. D: Appl. Phys.* **13** 839
[2] White T P, Lal N N and Catchpole K R 2014 *IEEE J. Photovolt.* **4** 208
[3] Mitroi M R, Ninulescu V and Fara L 2017 *Int. J. Photoenergy* **2017** 7284367
[4] Minami T, Nishi Y and Miyata T 2016 *Applied Physics Express* **9** 052301
[5] Wong T K S, Zhuk S, Masudy-Panah S and Dalapati G K 2016 *Materials* **9** 271
[6] Wang Y and Pierson J F 2021 *J. Phys. D: Appl. Phys.* **54** 263002
[7] Gan J, Hoye R L Z, Ievskaya Y, Vines L, Marin A T, MacManus-Driscoll J L and Monakhov E V 2020 *Sol. Energy Mater. Sol. Cells* **209** 110418
[8] Brandt R E, Young M, Park H H, Dameron A, Chua D, Lee Y S, Teeter G, Gordon R G and Buonassisi T 2014 *Appl. Phys. Lett.* **105** 263901
[9] Rizi M T, Abadi M H S and Ghaneii M 2018 *Optik* **155** 121
[10] Lee Y S, Chua D, Brandt R E, Siah S C, Li J V, Mailoa J P, Lee S W, Gordon R G and Buonassisi T 2014 *Adv. Mater.* **26** 4704–10
[11] Brandt R E, Lloyd M, Lee Y S, Siah S C and Buonassisi T 2013 *IEEE 39th Photovoltaic Specialists Conference (PVSC)* 846–8
[12] Meyer B *et al* 2013 The Physics of Copper Oxide (Cu2O) *Oxide Semiconductors* ed B G Svensson, S J Pearton and C Jagadish 88 (Amsterdam: Elsevier) 6 201 Semiconductors and Semimetals
[13] Scanlon D O and Watson G W 2011 *Phys. Rev. Lett.* **106** 186403
[14] Isseroff L Y and Carter E A 2013 *Chemistry of Materials* **25** 253
[15] Minami T, Nishi Y and Miyata T 2014 *Appl. Phys. Lett.* **105** 212104
[16] Nyborg M, Azarov A, Bergum K and Monakhov E 2021 *Thin Solid Films* **722** 138573
[17] Blood P and Orton J W 1992 *The Electrical Characterization of Semiconductors: Majority Carriers and Electron States* (London: Academic)
[18] Kittel C 2005 Point Defects *Introduction to Solid State Physics* 8th edn (New York: Wiley) 20
[19] Lee Y S, Winkler M T, Siah S C, Brandt R and Buonassisi T 2011 *Appl. Phys. Lett.* **98** 192115
[20] Frenkel J 1938 *Physical Review* **54** 647
[21] SILVACO® ATLAS™ User's Manual 2016